Dynamical Study of Femtosecond-Laser-Ablated Liquid-Aluminum Nanoparticles Using Spatiotemporally Resolved X-Ray-Absorption Fine-Structure Spectroscopy

Katsuya Oguri,* Yasuaki Okano,† Tadashi Nishikawa, and Hidetoshi Nakano

NTT Basic Research Laboratories, Nippon Telegraph and Telephone Corporation, 3-1 Morinosato Wakamiya, Atsugi, Kanagawa 243-0198, Japan

(Received 13 March 2007; published 18 October 2007)

We study the temperature evolution of aluminum nanoparticles generated by femtosecond laser ablation with spatiotemporally resolved x-ray-absorption fine-structure spectroscopy. We successfully identify the nanoparticles based on the L-edge absorption fine structure of the ablation plume in combination with the dependence of the edge structure on the irradiation intensity and the expansion velocity of the plume. In particular, we show that the lattice temperature of the nanoparticles is estimated from the L-edge slope, and that its spatial dependence reflects the cooling of the nanoparticles during plume expansion. The results reveal that the emitted nanoparticles travel in a vacuum as a condensed liquid phase with a lattice temperature of about 2500 to 4200 K in the early stage of plume expansion.

DOI: 10.1103/PhysRevLett.99.165003 PACS numbers: 52.38.Mf, 52.50.Jm, 61.10.Ht, 82.60.Qr

Nanometer-sized particle generation based on femtosecond laser ablation with various solid materials is of great interest as regards new material processing technology and the fundamental physics of the interaction between short-pulse lasers and matter [1–4]. A noteworthy characteristic of nanoparticle generation via femtosecond laser ablation is that the nanoparticles are produced as a result of material relaxation processes from the phase nonequilibrium between different states, which is achieved by the confinement of significant quantities of the laser energy deposited in the material before thermal conduction. This mechanism is completely different from conventional nanoparticle generation via nanosecond laser ablation [5]. However, little has yet been clarified about the fundamental physical behavior of material under such extreme conditions of temperature and pressure or its expansion dynamics that leads to nanoparticle generation. To date, mainly rough scenarios of nanoparticle generation have been proposed based on theoretical studies using molecular dynamics and hydrodynamics [6–10]. Although a few experimental approaches for measuring femtosecond laser ablation plumes have recently been described, experimental limitations meant that considerable uncertainty still remained with respect to even such fundamental information as the phase and temperature of nanoparticles. For instance, the nanoparticle temperature was estimated to be about 2300 K at 10 μs after femtosecond laser irradiation by using time-resolved optical emission spectroscopy [2,9], while rapid cooling to below 1440 K and the solidification of nanoparticles within 50 ps of laser irradiation was proposed based on an observation using time-resolved core-level photoemission spectroscopy [4,10].

With the above as the background, we developed a spatiotemporally resolved x-ray-absorption spectroscopy system that combines an ultrashort soft x-ray source based on femtosecond-laser-produced plasma and a Kirkpatrick-Baez microscope as an alternative tool for measuring a femtosecond laser ablation plume [11]. This system enabled us to measure the characteristic soft x-ray-absorption spectra of a femtosecond ablation plume of aluminum, but it was difficult to obtain detailed information about each ablation particle because of insufficient spectral resolution [12]. Here, we have significantly improved the spectral resolution of our previous system to overcome this prob-

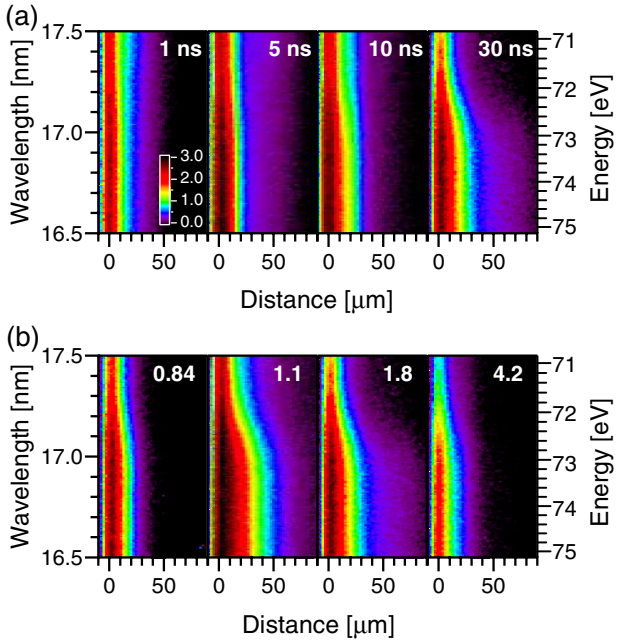

FIG. 1 (color online). Examples of spatially resolved soft-x-ray absorbance images of an aluminum plume. An absorbance image, μ_d, is defined as $\mu_d = \ln(I_0/I)$, where I_0 and I are the reference image without the plume absorption and the transmission spectrum with the plume absorption, respectively. (a) A temporal sequence of absorbance images at a laser irradiation intensity of 1.8×10^{14} W/cm^2. (b) Laser intensity dependence of the absorbance image of the aluminum plume at a delay time of 30 ns. The unit of intensity in the figure is 10^{14} W/cm^2.

lem, and have developed a spatiotemporally resolved x-ray-absorption fine-structure spectroscopy (STR-XAFS) system. By employing the new system to measure the femtosecond laser ablation process, we have successfully identified the nanoparticle component of the plume.

The STR-XAFS system has been developed based on certain major improvements made to the previous system. These consist of (i) a transmission grating with a higher spectral resolution, (ii) an x-ray charge-coupled device detector with a smaller pixel size, and (iii) soft x-ray generation with a double pulse excitation for enhancement of the x-ray emission [13]. The temporal, spatial, and spectral resolutions of this system were estimated to be about 30 ps, better than 12.5 μm, and greater than 180 at 72 eV, respectively. The sample was an aluminum ablation plume generated by focusing a 100-fs laser pulse onto a tape target.

Figure 1(a) shows examples of a temporal sequence of spatially resolved soft-x-ray absorbance images. In each absorbance image, we can observe a clear edge structure with a width about 1 eV near 72 eV (17.22 nm), which should correspond to one component that constitutes the plume. This energy range is very close to the energy of the L_{II} (73.15 eV) and L_{III} (72.71 eV) absorption edges of solid aluminum [14]. However, the sharpness of the edge structure was significantly reduced compared with that of the $L_{\mathrm{II,III}}$ absorption edge of solid aluminum (see Fig. 2). Since this feature is consistent with that of the K edge of liquid aluminum [15], the edge structure can be explained by the $L_{\mathrm{II,III}}$ absorption edge of the liquid component in the aluminum plume. The density of the liquid component near the surface region was estimated to be about 2×10^{-3} g/cm^3 by using the plume thickness approximated by the laser spot size and the mass absorption coefficient near the $L_{\mathrm{II,III}}$ absorption edge obtained by measuring solid aluminum. The large difference in density between the liquid component and a typical homogeneous liquid phase ($\sim$2.3 g/cm^3) [16] suggests that the liquid component corresponds to a collection of particles that preserve a condensed form. Therefore, the density of a single particle is likely to be comparable to that of the usual liquid phase while the average density of the probed region will be significantly low.

We also show the laser intensity dependence of the absorbance image in Fig. 1(b). From 8.4×10^{13} to 1.1×10^{14} W/cm^2, the absorption of the liquid component became strong because the increase in the laser irradiation intensity promoted laser ablation. In contrast, the liquid component absorption at an intensity of 1.1×10^{14} to 4.2×10^{14} W/cm^2 clearly became weak in spite of the large increase in the irradiation intensity. This observation is reminiscent of work reported by Eliezer *et al.* related to nanoparticle synthesis with femtosecond laser ablation under the same irradiation condition [3]. They confirmed the generation of aluminum nanoparticles ranging from about 10 to 500 nm in diameter as the result of irradiating

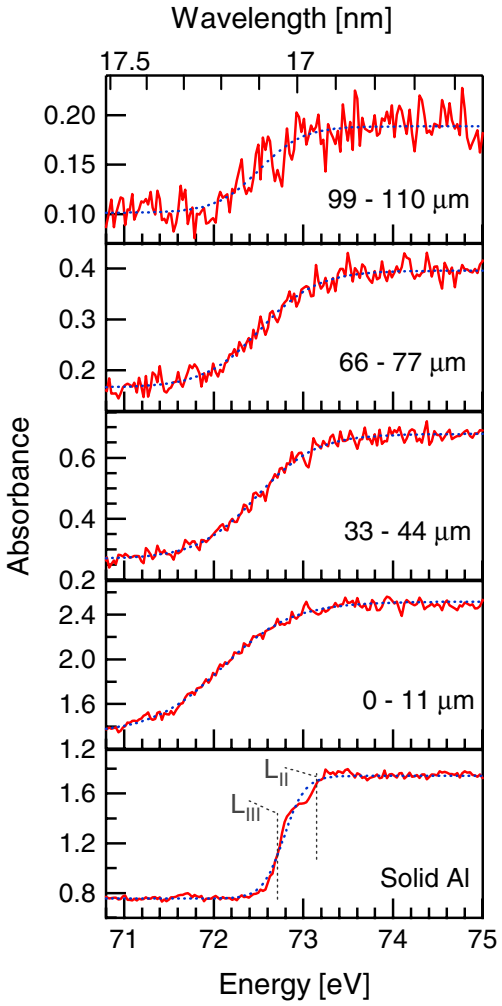

FIG. 2 (color online). Typical profiles of the near-edge absorbance spectrum of the aluminum nanoparticles at various distances from the surface and of solid aluminum with a thickness of 100 nm. Each profile is obtained by averaging the absorbance image in the 11 μm range at various distances. The laser irradiation intensity and the time delay are 1.8×10^{14} W/cm^2 and 30 ns, respectively. The blue dotted line shows the result of fitting to the edge slope with an FD distribution function. The nanoparticle lattice temperature was estimated by deconvoluting the broadening of the spectral resolution approximated by a Gaussian function from the fitting result.

aluminum foil with a 50-fs Ti:sapphire laser pulse with an intensity of 3×10^{12} to 5×10^{14} W/cm^2, and observed that the total number of particles per unit area decreased significantly at an intensity of 5×10^{14} W/cm^2, and no nanoparticle was generated at higher laser intensities. This experimental coincidence strongly suggests that the liquid component is most likely to correspond to aluminum nanoparticles in the liquid phase. In addition, Amoruso *et al.* estimated the average expansion velocity of aluminum nanoparticles in a femtosecond laser ablation plume to be about 1×10^3 m/s [9]. Since the expansion velocity of the liquid component was estimated to be roughly 1×10^3–2×10^3 m/s from Fig. 1, this coincidence as regards

the expansion velocity also strongly supports the view that the liquid component is identified as liquid aluminum nanoparticles.

Figure 2 shows typical profiles of the near-edge absorbance spectrum at various distances from the surface. The figure clearly shows that the liquid nanoparticle edge is less steep than that of solid aluminum, as we pointed out. The gradual decrease in the absorption of the nanoparticles with distance probably corresponds to the reduction in the average density in the plume while the condensed form of the nanoparticles is preserved. Furthermore, the figure also shows that the edge becomes gradually sharper as the distance increases. It is generally accepted that an x-ray-absorption edge shape can be understood in terms of a combination of the spectral resolution of the measurements, the intrinsic broadening induced by the lifetime of the initial core state, and the temperature effect on the Fermi surface [14,15]. The spectral resolution of our system was estimated to be about 0.44 eV near 73 eV from the energy separation of the L_{II} and L_{III} absorption edges of solid aluminum (the bottom profile in Fig. 2). On the other hand, the core lifetime broadening of the aluminum L_{II} and L_{III} levels was estimated to be of the order of 0.04 eV [17]. Therefore, the slope of the absorption edge observed in this study can be explained by the thermal broadening of the Fermi surface convoluted by the broadening caused by the spectral resolution. Since the electron distribution near the Fermi surface is known to obey the Fermi-Dirac (FD) distribution function, we can extract the electron temperature in the nanoparticles from an analysis of the slope of the absorption edge, which corresponds to $1/k_{\mathrm{B}}T$ where k_{B} and T represent the Boltzmann constant and electron temperature, respectively. Note that the electron temperature obtained from the analysis is almost equal to the lattice temperature of the nanoparticles because a laser-excited electron system typically heats an initially cooler lattice system to achieve thermal equilibrium after the laser irradiation on a time scale of 1 to 10 ps [8]. Therefore, we can obtain the average lattice temperature of many different nanoparticles because the measurements are on a 1-ns time scale in this study.

We obtained the spatial distribution of the lattice temperature of the nanoparticles in the plume [Fig. 3(a)]. The figure shows that the temperature decreases from ~4200 to ~2500 K as the nanoparticles travel further from the target surface. This suggests that the cooling of the nanoparticles proceeds in the plume front where the vacuum expansion is well promoted. In the dense region near the surface, therefore, the nanoparticle temperature should be relatively high. Figure 3(b) shows the temporal sequence of the nanoparticle temperature near the surface region from 0 to 11 μm. Owing to the limitation of the spatial resolution, the temperature is likely to reflect the cooler and faster nanoparticles that are dominantly distributed near the surface region in the early stages. Since the hotter and slower nanoparticles occupy the region afterwards, the temperature near the surface region seems to increase gradually with time.

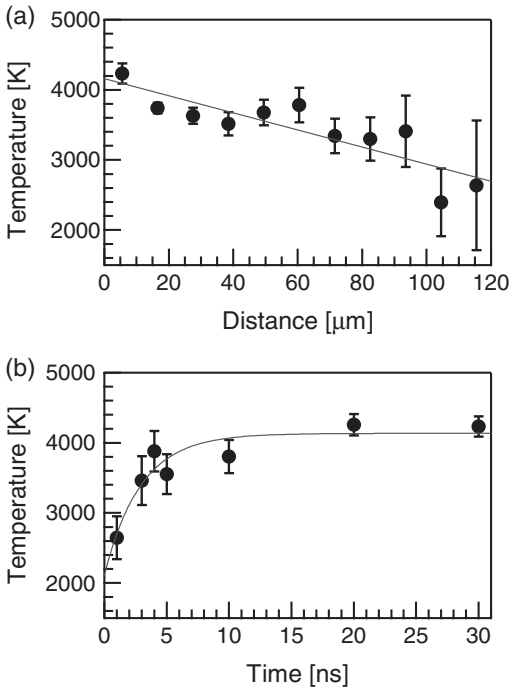

FIG. 3. Lattice temperature of the nanoparticles estimated from an analysis of the absorption edge slope. The solid curves are an eye guide. (a) The spatial distribution of the nanoparticle temperature in the plume at a time delay of 30 ns for an irradiation intensity of 1.8×10^{14} W/cm^2. (b) The temporal sequence of the nanoparticle temperature near the surface region from 0 to 11 μm for the same irradiation intensity.

Interestingly, we also observed a slight but clear edge shift to a lower energy than the solid aluminum $L_{\mathrm{II,III}}$ edge energy (Fig. 2). When we define the edge energy as the energy position at half of the edge height, the redshift ranges approximately from 0.2 to 0.6 eV. We plotted the edge energy of the nanoparticles as a function of the distance from the surface in Fig. 4. This figure shows that the redshift near the surface region is larger than that in the region far from the surface. Such a redshift in the x-ray-absorption edge was typically observed in early experimental studies, which reported a small redshift of 0.17 eV for the K edge on the solid-liquid phase transition in aluminum [15] and a large redshift of 0.7 to 7 eV in aluminum foil compressed by a laser-induced shock wave [18,19]. The absorption edge shift was generally explained by the sum of the blueshift that arises from the increase in the core-level ionization energy owing to the reduction in the shielding of the core electrons as a result of outer electron ionization, the redshift induced by the lowering of the continuum level due to the effect of high-density ions (continuum lowering), and the redshift caused by the decrease in the chemical potential of free electrons, based on the dense plasma model [18,19]. Although the early studies indicate that these physical factors are possibly related to

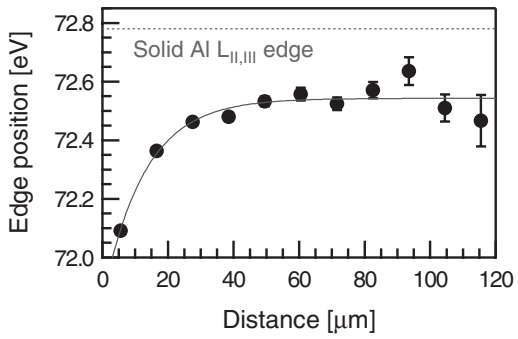

FIG. 4. The edge energy of the nanoparticles as a function of the distance from the surface. The laser irradiation intensity and the time delay are 1.8×10^{14} W/cm^2 and 30 ns, respectively.

the slight redshift of the nanoparticles observed in our study, the physical model of the redshift and its spatial dependence has not yet been clearly understood. Thus further investigations are required with regard to the edge shift of nanoparticles in an expanding femtosecond laser ablation plume.

Let us discuss the evolution dynamics of the nanoparticles according to recent theoretical studies [3,7–9]. When a femtosecond laser pulse with an intensity of about 10^{13} to 10^{14} W/cm^2 impulsively heats a solid surface, a molten layer with a lattice temperature of more than 10 000 K and a pressure of several tens of GPa is formed in the heated area as a result of isochoric heating [4,8]. It is proposed that nanoparticles are generated during the expansion of the molten layer via photomechanical fragmentation and phase explosion for laser irradiation fluences above and near the ablation threshold, respectively [7,8]. In this study, the laser irradiation fluences ranged above the ablation threshold of aluminum (about 0.1 J/cm^2), thus suggesting that we observed a collection of nanoparticles that were predominantly generated by photomechanical fragmentation. Photomechanical fragmentation is generally a process where an initially homogeneous molten layer decomposes into an inhomogeneous collection of liquid nanoparticles and gaseous atoms above the critical temperature (about 6000 K for aluminum [3,9]). Therefore, it is reasonable that the nanoparticle lattice temperature on a 10-ns time scale obtained in Fig. 3 ranges from the critical temperature to the nanoparticle temperature in a previously measured well-expanded plume (e.g., about 2300 K at 10 μs for silicon nanoparticles [2]). In conclusion, our results clearly showed that the nanoparticles travel in a vacuum as a hot liquid phase in the early stages of the expansion of the femtosecond laser ablation plume.

In summary, we successfully identified liquid nanoparticles in a femtosecond laser ablation plume with spatiotemporally resolved XAFS spectroscopy. The results strongly suggest that the emitted nanoparticles travel in a vacuum as a hot liquid phase with a temperature of about 2500 to 4200 K. When further improvements are achieved in spatial ($\sim$1 μm) and temporal ($\sim$1 ps) resolution in the near future, the STR-XAFS technique will be used to provide experimental evidence for its mechanism.

We thank Dr. Y. Furukawa (Osaka University) for helpful discussions. This work was partly financed by the Ministry of Education, Culture, Sports, Science and Technology of Japan under Grant-in-Aid for Scientific Research No. 16032219.

*oguri@nttbrl.jp
†Present address: Institute of Laser Engineering, Osaka University, 2-6 Yamadaoka Suita, Osaka, Osaka 565-0871, Japan.

[1] J. Perrière, E. Millon, W. Seiler, C. Boulmer-Leborgne, V. Craciun, O. Albert, J. C. Loulergue, and J. Etchepare, J. Appl. Phys. **91**, 690 (2002).
[2] S. Amoruso, R. Bruzzese, N. Spinelli, R. Velotta, M. Vitiello, X. Wang, G. Ausanio, V. Iannotti, and L. Lanotte, Appl. Phys. Lett. **84**, 4502 (2004).
[3] S. Eliezer, N. Eliaz, E. Grossman, D. Fisher, I. Gouzman, Z. Henis, S. Pecker, Y. Horovitz, M. Fraenkel, S. Maman, and Y. Lereah, Phys. Rev. B **69**, 144119 (2004).
[4] T. E. Glover, G. D. Ackerman, A. Belkacem, P. A. Heimann, Z. Hussain, R. W. Lee, H. A. Padmore, C. Ray, R. W. Schoenlein, W. F. Steele, and D. A. Young, Phys. Rev. Lett. **90**, 236102 (2003).
[5] P. R. Willmott and J. R. Huber, Rev. Mod. Phys. **72**, 315 (2000).
[6] F. Vidal, T. W. Johnston, S. Laville, O. Barthélemy, M. Chaker, B. Le Drogoff, J. Margot, and M. Sabsabi, Phys. Rev. Lett. **86**, 2573 (2001).
[7] D. Perez and L. J. Lewis, Phys. Rev. Lett. **89**, 255504 (2002).
[8] P. Lorazo, L. J. Lewis, and M. Meunier, Phys. Rev. B **73**, 134108 (2006).
[9] S. Amoruso, R. Bruzzese, M. Vitiello, N. N. Nedialkov, and P. A. Atanasov, J. Appl. Phys. **98**, 044907 (2005).
[10] T. E. Glover, G. D. Ackerman, R. W. Lee, and D. A. Young, Appl. Phys. B **78**, 995 (2004).
[11] Y. Okano, K. Oguri, T. Nishikawa, and H. Nakano, Rev. Sci. Instrum. **77**, 046105 (2006).
[12] Y. Okano, K. Oguri, T. Nishikawa, and H. Nakano, Appl. Phys. Lett. **89**, 221502 (2006).
[13] H. Nakano, T. Nishikawa, H. Ahn, and N. Uesugi, Appl. Phys. Lett. **69**, 2992 (1996).
[14] C. Gähwiller and F. C. Brown, Phys. Rev. B **2**, 1918 (1970).
[15] C. F. Hague, Phys. Rev. B **25**, 3529 (1982).
[16] M. J. Assael, K. Kakosimos, R. M. Banish, J. Brillo, I. Egry, R. Brooks, P. N. Quested, K. C. Mills, A. Nagashima, Y. Sato, and W. A. Wakeham, J. Phys. Chem. Ref. Data **35**, 285 (2006).
[17] P. H. Citrin, G. K. Wertheim, and M. Schlüter, Phys. Rev. B **20**, 3067 (1979).
[18] J. Workman, M. Nantel, A. Maksimchuk, and D. Umstadter, Appl. Phys. Lett. **70**, 312 (1997).
[19] J. Al-Kuzee, T. A. Hall, and H-D. Frey, Phys. Rev. E **57**, 7060 (1998).